BIOCHEMISTRY
including biophysical chemistry & molecular biology

Article

pubs.acs.org/biochemistry

Energetic Coupling between Ligand Binding and Dimerization in *Escherichia coli* Phosphoglycerate Mutase

Nathan W. Gardner,[†,‡] Lyman K. Monroe,[§] Daisuke Kihara,[§,∥] and Chiwook Park*[,†,‡,⊥]

[†]Department of Medicinal Chemistry and Molecular Pharmacology, [‡]Interdisciplinary Life Science Graduate Program, [§]Department of Biological Sciences, [∥]Department of Computer Science, and [⊥]Bindley Bioscience Center, Purdue University, West Lafayette, Indiana 47907, United States

Supporting Information

ABSTRACT: Energetic coupling of two molecular events in a protein molecule is ubiquitous in biochemical reactions mediated by proteins, such as catalysis and signal transduction. Here, we investigate energetic coupling between ligand binding and folding of a dimer using a model system that shows three-state equilibrium unfolding of an exceptional quality. The homodimeric *Escherichia coli* cofactor-dependent phosphoglycerate mutase (dPGM) was found to be stabilized by ATP in a proteome-wide screen, although dPGM does not require or utilize ATP for enzymatic function. We investigated the effect of ATP on the thermodynamic stability of dPGM using equilibrium unfolding. We found that, in the absence of ATP, dPGM populates a partially unfolded, monomeric intermediate during equilibrium unfolding. However, addition of 1.0 mM ATP drastically reduces the population of the intermediate by selectively stabilizing the native dimer. Using a computational ligand docking method, we predicted ATP binds to the active site of the enzyme using the triphosphate group. By performing equilibrium unfolding and isothermal titration calorimetry with active-site variants of dPGM, we confirmed that active-site residues are involved in ATP binding. Our findings show that ATP promotes dimerization of the protein by binding to the active site, which is distal from the dimer interface. This cooperativity suggests an energetic coupling between the active site and the dimer interface. We also propose a structural link to explain how ligand binding to the active site is energetically coupled with dimerization.

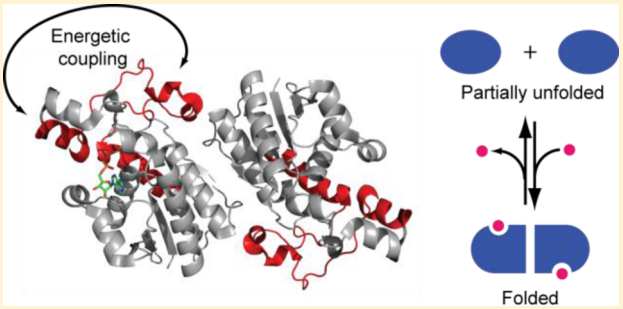

Cooperativity between two events occurring at two distant sites is a salient feature of protein molecules. Protein folding is a cooperative process in which a group of structural units in a protein fold or unfold simultaneously.[1] Because of their cooperative nature, conformational energy landscapes of proteins are composed of discrete partially unfolded forms rather than a continuum of possible conformations.[2−4] Ligand binding events at two different binding sites in a protein are frequently cooperative; binding of one ligand positively or negatively influences binding of the other ligand. The cooperative binding of two ligands is the basis of allostery,[5,6] which is commonly observed in many aspects of cellular processes, such as catalysis and signal transduction. The fundamental principle of cooperativity is the same whether it is observed in ligand binding or in protein folding.[7] Ligand binding as well as folding/unfolding of a region modulates the conformational energy landscape of a protein. The change in the energy and the population of various conformations results in the changes in macroscopic structural properties in proteins. The structural changes can be as subtle as changes in side-chain dynamics or as drastic as folding of unstructured domains.[5] Understanding the energetic basis of the cooperativity in protein structure is one of the most important challenges in biochemistry.

From our previous proteomics study, we identified a protein that shows a remarkable energetic coupling between ligand binding and folding. Previously, we conducted an energetics-based proteome screen to identify ATP-binding proteins in the *Escherichia coli* proteome.[8,9] This proteome screen exploits the fact that ligand binding stabilizes proteins.[10−12] We subjected proteins in an *E. coli* lysate to urea unfolding in the presence and absence of 1.0 mM ATPγS and compared the amount of proteins that remain intact after pulse proteolysis.[8,9] Pulse proteolysis is a way to monitor protein unfolding by selectively digesting the unfolded proteins through a brief incubation with a nonspecific protease.[13] Different from traditional methods based on spectroscopy or calorimetry, pulse proteolysis allows us to study unfolding of many proteins simultaneously on a proteomic scale.[8,9,14] At 2.0 M urea, cofactor-dependent phosphoglycerate mutase (dPGM) was fully digested without ATP, but a significant population of the protein remained intact in the presence of 1.0 mM ATPγS.[8] *E. coli* dPGM is a homodimer consisting of 249-amino acid subunits with a molecular weight of 28.4 kDa. Interestingly, dPGM does not

Received: September 4, 2015
Revised: February 24, 2016

DOI: 10.1021/acs.biochem.5b00980
Biochemistry XXXX, XXX, XXX−XXX

require ATP for its enzyme activity. However, we confirmed the stabilization of dPGM in the presence of 1.0 mM ATP by performing pulse proteolysis with purified dPGM.[15] Later, the Fitzgerald group reported that ATP also stabilizes *Saccharomyces cerevisiae* dPGM in an energetics-based proteome screen similar to ours.[16]

Phosphoglycerate mutases (EC 5.4.2.11) catalyze the essential isomerization reaction between 3-phosphoglycerate and 2-phosphoglycerate in the glycolysis and gluconeogenesis pathways. Most vertebrates, yeast, and bacteria possess a cofactor-dependent phosphoglycerate mutase (dPGM) that must be activated by the cofactor 2,3-bisphosphoglycerate (2,3-BPG).[17] In the activating reaction, dPGM serves as a phosphatase (EC 3.1.3.13) for 2,3-BPG and converts 2,3-BPG into 2-phosphoglycerate or 3-phosphoglycerate while retaining a phosphate group on an active-site histidine residue. In the isomerization reaction, the phosphate group on the phosphohistidine of the activated enzyme is transferred to 2-phosphoglycerate or 3-phosphoglycerate, and the resulting 2,3-BPG is used to phosphorylate the histidine residue. Through this process, dPGM shuttles a phosphate group between 3-phosphoglycerate and 2-phosphoglycerate.

To quantitatively assess the effect of ATP on the stability of this enzyme, we monitored urea-induced equilibrium unfolding of *E. coli* dPGM using fluorescence and circular dichroism. In the absence of ATP, equilibrium unfolding of dPGM reveals two well-separated transitions with an equilibrium intermediate, indicating that dPGM unfolds in a three-state manner. Interestingly, we found that the equilibrium intermediate disappears in the presence of ATP; dPGM unfolds in a two-state manner without any observable equilibrium intermediate upon binding to ATP. Realizing that this protein is an excellent model system for understanding the molecular mechanism for the energetic coupling between ligand binding and folding, we decided to investigate how ATP binding promotes dimerization of dPGM. We employed both experimental and computational approaches to dissect the molecular details of the interaction between dPGM and ATP and the energetic coupling between ATP binding and dPGM folding. On the basis of our experimental data, we propose a structural model for the cooperativity between folding of the active site and the dimer interface.

EXPERIMENTAL PROCEDURES

Preparation of Purified dPGM. We overexpressed dPGM in *E. coli* BL21(DE3)pLysS cells under the control of the T7 promoter as described previously.[8] After resuspending the harvested cells in 20 mM TrisHCl-NaOH buffer (pH 8.0) containing 10 mM EDTA, we lysed the cells by sonication. We collected the supernatant after centrifugation and sterilized the lysate via filtration with a 0.45 μm filter. We loaded the lysate into a DEAE-sepharose FF column (GE Healthcare Life Sciences, Piscataway, NJ) pre-equilibrated with 20 mM TrisHCl-NaOH buffer (pH 8.0). Bound proteins were eluted with a linear NaCl gradient from 0.10 to 0.35 M. We then pooled the fractions containing dPGM and dialyzed them overnight against 20 mM TrisHCl-NaOH buffer (pH 8.0). We further purified the dialyzed solution using a Source 15Q column on an ÄKTA FPLC system (GE Healthcare Life Sciences, Pittsburgh, PA). Bound protein was eluted with a linear NaCl gradient from 0 to 0.25 M. We checked the purity of dPGM by sodium dodecyl sulfate−polyacrylamide gel electrophoresis (SDS−PAGE). We concentrated the purified protein with a Centriprep 10K centrifugal filter (EMD Millipore, Billerica, MA) and determined the concentration of dPGM by absorbance at 280 nm using an extinction coefficient of 56380 M^{-1} cm^{-1}, which is estimated from the amino acid composition.[18]

QuikChange site-directed mutagenesis kits (Agilent Technologies, Santa Clara, CA) were used to produce all dPGM variants. The sequence of each variant was verified at the Purdue Genomics Core Facility (West Lafayette, IN). All dPGM variants were purified through the two rounds of anion exchange chromatography as described above.

Equilibrium Unfolding and Analysis. We prepared 30 μg/mL dPGM (~1.0 μM) in 20 mM TrisHCl-NaOH buffer (pH 8.0) containing varying concentrations of urea (0−5 M). We investigated the equilibrium unfolding of dPGM under a low-ionic strength condition where the application of the three-state model was most reliable and the effect of ATP was maximal (data not shown). The absolute urea concentrations were determined from the refractive index.[19] Additional ligands varied on an experimental basis. The samples were equilibrated overnight prior to spectroscopy. The unfolding of dPGM was monitored by intrinsic tryptophan fluorescence or circular dichroism (CD). Fluorescence emission spectra were recorded from 320 to 400 nm with a FluoroMax-3 fluorimeter (Horiba Jobin Yvon, Edison, NJ) using an excitation wavelength of 280 nm. Changes in molar ellipticity were monitored at 222 nm with a J-815 CD spectrometer (JASCO, Easton, MD).

To analyze equilibrium unfolding by fluorescence, we first calculated the intensity-weighted average wavelength (IWAW):

$$\mathrm{IWAW} = \frac{\sum \lambda \times I}{\sum I} \tag{1}$$

where λ is the emission wavelength and I is the fluorescence intensity. Unlike the raw fluorescence intensity data, IWAW is not sensitive to variations in protein concentration and provides a reliable measure of protein unfolding.

Equilibrium unfolding data were fit to a three-state model with a monomer intermediate (Scheme 1).[20,21] The equilibrium

Scheme 1

$$\mathrm{N_2} \overset{K_1}{\rightleftarrows} 2\mathrm{I} \overset{K_2}{\rightleftarrows} 2\mathrm{U}$$

constants are defined as $K_1 = [\mathrm{I}]^2/[\mathrm{N_2}]$ and $K_2 = [\mathrm{U}]/[\mathrm{I}]$. By the linear extrapolation method,[22] the dependence of the equilibrium constants on urea concentration is expressed as

$$K_1 = \exp\left(\frac{m_{\mathrm{I-N}}D - \Delta G_{\mathrm{I-N}}^{\circ}}{RT}\right) \tag{2}$$

$$K_2 = \exp\left(\frac{m_{\mathrm{U-I}}D - \Delta G_{\mathrm{U-I}}^{\circ}}{RT}\right) \tag{3}$$

where D is the urea concentration, $\Delta G_{\mathrm{I-N}}^{\circ}$ is the free energy difference between N_2 and 2I at 0 M urea, and $\Delta G_{\mathrm{U-I}}^{\circ}$ is the free energy difference between U and I at 0 M urea. The $m_{\mathrm{I-N}}$ and $m_{\mathrm{U-I}}$ values are the dependencies of $\Delta G_{\mathrm{I-N}}^{\circ}$ and $\Delta G_{\mathrm{U-I}}^{\circ}$, respectively, on urea concentration. The spectroscopic signal, Y_0, is expressed as a summation of the contribution of each state:

$$Y_0 = Y_{\mathrm{N}}f_{\mathrm{N}} + Y_{\mathrm{I}}f_{\mathrm{I}} + Y_{\mathrm{U}}f_{\mathrm{U}} \tag{4}$$

DOI: 10.1021/acs.biochem.5b00980
Biochemistry XXXX, XXX, XXX−XXX

where Y_N, Y_I, and Y_U are the spectroscopic signals of N_2, I, and U, respectively, and f_N, f_I, and f_U are the fractions of the monomeric unit in N_2, I, and U, respectively ($f_N + f_I + f_U = 1$). We expressed f_N, f_I, and f_U as functions of K_1, K_2, and P_t, the total protein concentration in the monomeric unit ($P_t = 2[N_2] + [I] + [U]$), as described elsewhere.[21] We determined m_{I-N}, m_{U-I}, ΔG_{I-N}°, and ΔG_{U-I}° by fitting equilibrium unfolding data with eq 4 using OriginPro 8.5.1 (OriginLab, Northampton, MA). For global fitting of multiple equilibrium unfolding data sets, we reduced parameters by sharing the spectroscopic signals for the intermediate state and unfolded state, both *m*-values, and P_t among all data sets. For global fittings in Figures 3 and 5, the spectroscopic signals were normalized to obtain the relative signal, Y_R, which is defined as

$$Y_R = \frac{Y_0 - Y_N}{Y_U - Y_N} \tag{5}$$

where Y_0 is the spectroscopic signal at a given urea concentration.

When the stability of dPGM was determined in the presence of a ligand, we calculated the dissociation equilibrium constant K_d from the increase in stability ($\Delta\Delta G_{unf}^\circ$) using the following relationship:[23]

$$\Delta\Delta G_{unf}^\circ = RT \ln\left(1 + \frac{[L]}{K_d}\right) \tag{6}$$

where K_d is the dissociation equilibrium constant and [L] is the ligand concentration.

Chemical Cross-Linking. To monitor dissociation of the dPGM dimer during equilibrium unfolding, we chemically cross-linked the dimer using bis(succinimidyl) penta(ethylene glycol) [BS(PEG)$_5$] (Thermo Fisher Scientific, Waltham, MA) at varying concentrations of urea. We dialyzed a concentrated dPGM solution against 20 mM HEPES-HCl buffer (pH 8.0). Using the dialyzed dPGM solution, we prepared 0.20 mg/mL dPGM in 20 mM HEPES-HCl buffer (pH 8.0) with varying concentrations of urea (0−5 M). We initiated cross-linking by adding BS(PEG)$_5$ to a final concentration of 2.0 mM. After incubating the reaction mixture at 25 °C for 1 h, we mixed 80 μL of each sample with 20 μL of 5-fold concentrated SDS−PAGE sample buffer. We analyzed the SDS−PAGE samples with a 15% polyacrylamide gel. After staining the SDS−PAGE gel with Sypro Red Protein Gel Stain (Life Technologies, Grand Island, NY), we imaged the gel with a Typhoon scanner (GE Healthcare Life Sciences, Pittsburgh, PA) and quantified the band intensities using ImageJ (http://imagej.nih.gov/ij).

Size Exclusion Chromatography. We conducted size exclusion chromatography using a TSKgel G3000SWxL column (TOSOH Bioscience LLC, King of Prussia, PA) with a column volume of ∼14.3 mL. The mobile phase was 20 mM TrisHCl-NaOH buffer (pH 8.0) containing 50 mM NaCl and 0 or 2.5 M urea. We prepared 30 μg/mL dPGM in a respective mobile phase. For each run, we injected 50 μL of a dPGM solution into the column and ran the column at a rate of 0.5 mL/min while the absorbance at 280 nm was recorded.

ATP Docking Using Glide. Docking of ATP to dPGM was conducted with the Maestro software suite (Schrödinger LLC, New York, NY). The ATP ligand was prepared for docking using the LigPrep plugin included in Maestro. ATP was docked to inactive dPGM [Protein Data Bank (PDB) entry 1E59] using Glide (grid-based ligand docking with energetics) docking.[24] For docking, the OPLS_2005 force field was used and ionization states for ATP were determined under pH 8.0 ± 2.0 using Epik. A cubic docking grid was generated to fit the entire dPGM monomer so that the binding location was unbiased. Docking was performed using Glide's XP (extra precision) setting with the ligand treated flexibly. From the docking run, the top 4 scoring ATP poses were retained.

Circular Dichroism. CD spectra spanning 190−250 nm were recorded on a JASCO J-815 CD spectrometer (JASCO, Easton, MD). dPGM samples were prepared from 10-fold dilutions of a concentrated protein stock. The concentrations of dPGM were determined by the absorbance at 280 nm. Samples were equilibrated at room temperature for at least 2 h prior to the measurement.

Isothermal Titration Calorimetry. All dPGM variants were prepared at 42 μM (1.2 mg/mL) and dialyzed against 20 mM TrisHCl-NaOH (pH 8.0) for ITC. After dialysis, the dPGM concentration was determined by the absorbance at 280 nm. ATP (Sigma-Aldrich, St. Louis, MO) was prepared at a concentration of 0.40 mM in dialysis buffer. To monitor binding of ATP to dPGM, heat evolution was monitored with a MicroCal iTC200 calorimeter (GE Healthcare Life Sciences, Pittsburgh, PA) upon ATP titration. ATP was titrated through 21 injections of 0.40 mM ATP with 3 min intervals. The resulting thermograms were automatically integrated by NITPIC[25] and fit with a model of 1:1 binding using SEDPHAT (https://sedfitsedphat.nibib.nih.gov).[26] The fitted curves were plotted using GUSSI (http://biophysics.swmed.edu/MBR/software.html).

RESULTS

Equilibrium Unfolding of dPGM in the Presence and Absence of ATP. We monitored equilibrium unfolding of dPGM in the absence and presence of 1.0 mM ATP by intrinsic tryptophan fluorescence (Figure 1A). From the fluorescence emission spectrum at each urea concentration, we calculate one intensity-weighted average wavelength (IWAW). When dPGM unfolds and its tryptophans become more solvent-exposed, IWAW shifts to longer wavelengths. Immediately apparent in Figure 1A is the fact that equilibrium unfolding of dPGM occurs in a three-state manner in the absence of ATP. A shoulder occurs between 2 and 3 M urea with an IWAW value of ∼355 nm, signifying that an intermediate state with properties distinct from those of the native and unfolded states is populated. The first unfolding transition has a transition midpoint (C_m) of ∼1.4 M urea and occurs with a signal change that is ∼70% of the total change in fluorescence. The second unfolding transition has a C_m value of ∼3.5 M urea. We also monitored the equilibrium unfolding of dPGM by circular dichroism (Figure S1 of the Supporting Information). The two transitions observed by CD occur with the same C_m values as those observed by fluorescence, suggesting that we are observing the same and only equilibrium intermediate. The first transition occurs with 35% of the total change in CD signal upon global unfolding. Unfolding to the intermediate state appears to involve some loss of secondary structure as well as significant changes in the environment around tryptophan residues.

In the presence of 1.0 mM ATP, equilibrium unfolding of dPGM occurs in only one apparent transition with a C_m of ∼3.6 M urea without any indication of an equilibrium intermediate (Figure 1A). The addition of 1.0 mM ATP not only stabilizes dPGM dramatically but also suppresses accumulation of the equilibrium intermediate. Because of strong UV absorption by

DOI: 10.1021/acs.biochem.5b00980
Biochemistry XXXX, XXX, XXX−XXX

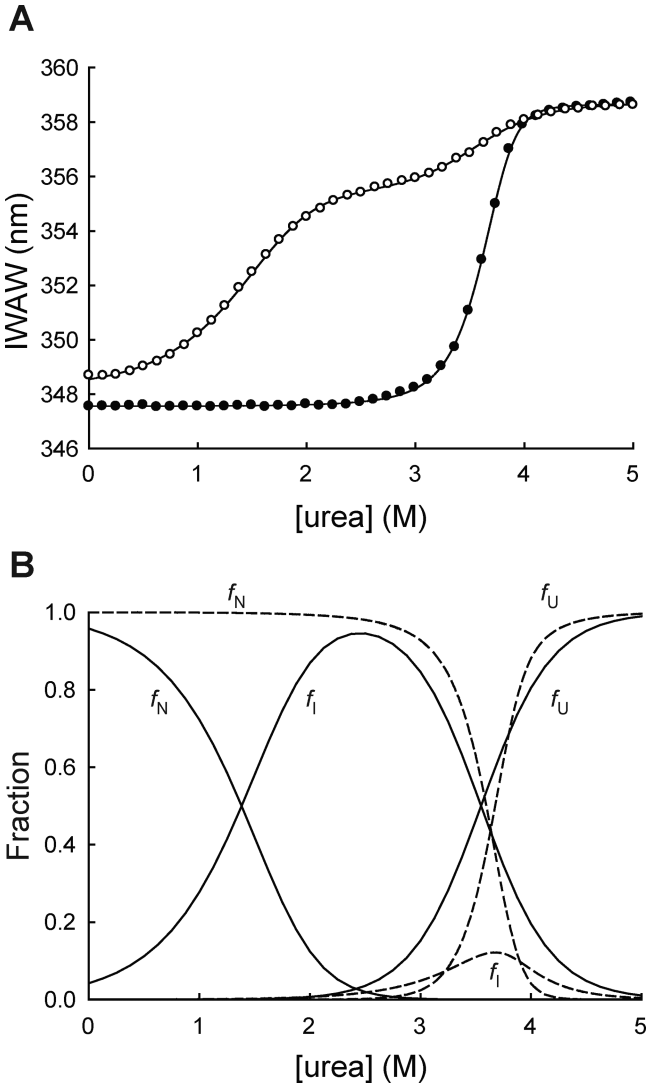

Figure 1. Effect of ATP on the equilibrium unfolding of dPGM. (A) Equilibrium unfolding of 0.030 mg/mL dPGM was monitored by tryptophan fluorescence in the absence (○) and presence (●) of 1.0 mM ATP. (B) Populations of native, intermediate, and unfolded dPGM during equilibrium unfolding. The fraction of native (f_N), intermediate (f_I), and unfolded (f_U) dPGM for 0.030 mg/mL dPGM in the absence (—) and presence (– – –) of 1.0 mM ATP was calculated with the fitting parameters listed in Table 1.

ATP, equilibrium unfolding of dPGM in the presence of 1.0 mM ATP could not be monitored by CD.

Oligomeric State of the Equilibrium Intermediate. Developing a model for analyzing the equilibrium unfolding of a dimeric protein with an equilibrium intermediate requires knowledge of whether the intermediate is a monomer or a dimer. First, we investigated the oligomeric state of the intermediate of dPGM through the dependence of equilibrium unfolding on protein concentration. As the protein concentration is increased, dimeric states should be stabilized due to Le Chatelier's principle. Therefore, a transition that shows a dependence on the protein concentration involves a change in oligomeric state from dimer to monomer. When we monitored equilibrium unfolding of dPGM with three different concentrations of dPGM (10, 30, and 100 μg/mL), we clearly observed that, as the protein concentration increases, the apparent C_m value of the first transition gradually increases, as well (Figure 2A). The second transition does not exhibit any observable dependency on protein concentration. We also

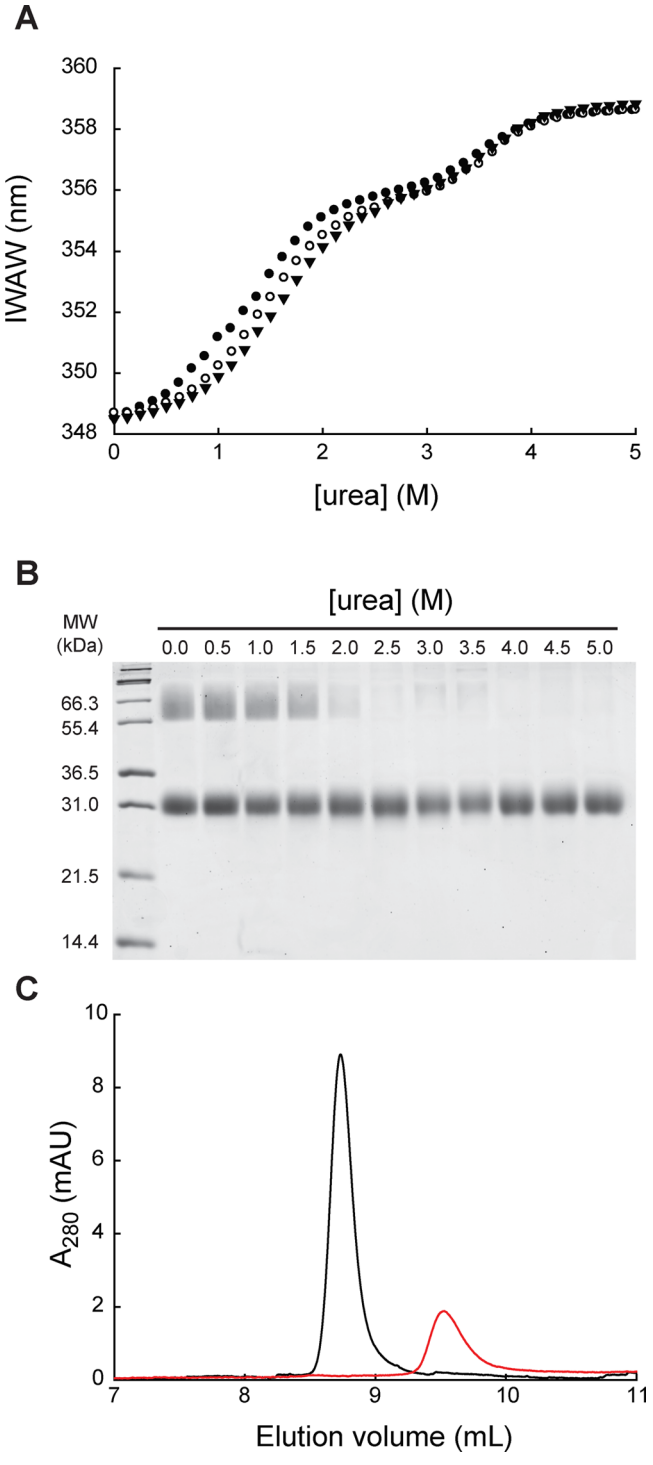

Figure 2. Oligomeric state of the equilibrium intermediate. (A) Equilibrium unfolding of dPGM at 0.01 (●), 0.03 (○), and 0.10 mg/mL (▼) monitored by tryptophan fluorescence. Intensity-weighted average wavelengths (IWAWs) were calculated from fluorescence emission spectra. (B) Chemical cross-linking of 0.20 mg/mL dPGM in the presence of 0–5 M urea. MW indicates the molecular weights of standard proteins in the protein ladder. (C) Elution profiles of 0.03 mg/mL dPGM from size exclusion chromatography at 0 M urea (black) and 2.5 M urea (red). Elution was monitored by the absorbance at 280 nm (A_{280}).

DOI: 10.1021/acs.biochem.5b00980
Biochemistry XXXX, XXX, XXX–XXX

Table 1. Thermodynamic Parameters of dPGM in the Presence and Absence of ATP

probe	[ATP] (mM)	ΔG_{I-N}° (kcal/mol)	m_{I-N} (kcal mol^{-1} M^{-1})	ΔG_{U-I}° (kcal/mol)	m_{U-I} (kcal mol^{-1} M^{-1})	ΔG_{U-N}° (kcal/mol)
fluorescence	0	11.5 ± 0.1	2.40 ± 0.06	6.6 ± 0.3	1.86 ± 0.09	24.7 ± 0.6
	1.0	18.5 ± 0.2	–	6.0 ± 0.4	–	30.5 ± 0.8
CD	0	11.9 ± 0.2	2.3 ± 0.1	6.2 ± 0.3	1.80 ± 0.07	24.3 ± 0.6

monitored equilibrium unfolding of 20, 30, and 100 μg/mL dPGM by circular dichroism (CD), which confirmed the concentration dependence of the first transition (Figure S2 of the Supporting Information). The concentration dependence of equilibrium unfolding best supports a monomer intermediate.

We further examined the oligomeric state of the intermediate by chemical cross-linking with $BS(PEG)_5$, which reacts selectively with amine groups. After dPGM was incubated with $BS(PEG)_5$ in varying concentrations of urea (0−5 M), the cross-linked samples were visualized by SDS−PAGE (Figure 2B). Without urea, the dPGM dimer and monomer bands are both visible and migrate with apparent molecular weights of ∼60 and ∼30 kDa, respectively. The dimer band intensity decreases as the urea concentration is increased and disappears at 2.5 M urea. For facile detection, we used in this experiment 0.20 mg/mL dPGM, which is 2-fold greater than the highest concentration we used in the equilibrium unfolding study. Still, it is obvious that the disappearance of the dimer band is coincidental with the first transition in the equilibrium unfolding of dPGM. This result confirms that the equilibrium intermediate is a monomer.

We also monitored the change in the hydrodynamic radius of 30 μg/mL dPGM by size exclusion chromatography under conditions favoring the native state (0 M urea) and the intermediate state (2.5 M urea) (Figure 2C). Without urea, one sharp peak is observed at an elution volume of 8.7 mL. In the presence of 2.5 M urea, one peak is observed at an elution volume of 9.5 mL. The change in the elution volume indicates that dPGM has a smaller radius at 2.5 M urea than at 0 M urea, suggesting that the intermediate is a monomer. The peak at 2.5 M urea is broader and, therefore, has a peak height smaller than that of the peak at 0 M urea. Exchange between multiple conformations may cause the peak broadening observed at 2.5 M urea. The results of the concentration dependence of equilibrium unfolding, chemical cross-linking, and size exclusion experiments all support a monomer intermediate. With the oligomeric state determined, we use a three-state model with a monomer intermediate (Scheme 1) to analyze the equilibrium unfolding of dPGM.

Effect of ATP on the Thermodynamic Stability of dPGM. Using the model shown in Scheme 1, we quantified the effect of ATP on the equilibrium unfolding of dPGM (Figure 1 and Table 1). We fit globally the fluorescence-monitored equilibrium unfolding data in the presence and absence of 1.0 mM ATP with the three-state model, despite the apparent two-state transition in equilibrium unfolding of dPGM in the presence of ATP. In the global fit, we reduced fitting parameters by sharing intermediate state and unfolded state signals, *m*-values, and the total protein concentration. In the absence of ATP, the free energy associated with the first transition ($N_2 \rightarrow 2I$; ΔG_{I-N}°) and the second transition ($I \rightarrow U$; ΔG_{U-I}°) were determined to be 11.5 ± 0.1 and 6.6 ± 0.3 kcal/mol, respectively (Table 1). Independent curve fitting of the equilibrium unfolding of dPGM monitored by CD yielded similar values (Table 1 and Figure S1 of the Supporting Information). Note that the first transition is the unfolding of the dimer and that ΔG_{I-N}° is the free energy change under the standard condition where both $[N_2]$ and [I] are 1 M. To get a better sense of the stability of the protein under our experimental condition (1.0 μM dPGM), we determined f_N, f_I, and f_U using the equilibrium parameters from the curve fitting (Figure 1B). According to the calculation, the effective stability (ΔG_{eff}),[27] which is defined as $-RT \ln[(1 - f_N)/f_N]$ at a given protein concentration, is only 1.9 kcal/mol under native conditions; one in 25 monomeric units adopt a non-native conformation (Figure 1B). ATP at a concentration of 1.0 mM increases ΔG_{I-N}° by 7.0 ± 0.2 kcal/mol, which corresponds to an increase in stability of 3.5 kcal/mol per monomeric unit. The effect of 1.0 mM ATP on ΔG_{U-I}° was insignificant (0.6 kcal/mol). In the presence of 1.0 mM ATP, the effective stability of 1.0 μM dPGM is increased to 5.4 kcal/mol. The resulting effect of ATP is that only one in 8600 monomeric units adopts a non-native conformation under native conditions (Figure 1B). Further, in the absence of ATP, the intermediate reaches a maximal fraction of just over 0.94 around 2.5 M urea. In the presence of 1.0 mM ATP, the intermediate reaches a maximal fraction of only 0.12 around 3.7 M urea. ATP dramatically suppresses accumulation of the equilibrium intermediate. Therefore, our analysis strongly suggests that ATP selectively binds to the native dimer and not to the monomeric intermediate.

The dependence of ΔG_{I-N}° and ΔG_{U-I}° on urea concentration, m_{I-N} and m_{U-I}, respectively, signifies that both transitions involve substantial unfolding. The *m*-value is proportional to the change in a protein's solvent-accessible surface area during unfolding.[28] From the global fitting, we find that m_{I-N} is 2.40 kcal mol^{-1} M^{-1} and m_{U-I} is 1.86 kcal mol^{-1} M^{-1}. The total *m*-value for global unfolding, m_{U-N}, is 3.06 kcal mol^{-1} M^{-1} per monomeric unit ($m_{U-N} = m_{I-N}/2 + m_{U-I}$), which is in agreement with the *m*-value predicted for a dPGM monomer based on the number of residues (3.2 kcal mol^{-1} M^{-1}).[28] Curve fitting of the equilibrium unfolding of dPGM monitored by CD produced similar *m*-values: m_{I-N} of 2.3 kcal mol^{-1} M^{-1}, m_{U-I} of 1.80 kcal mol^{-1} M^{-1}, and m_{U-N} of 2.95 kcal mol^{-1} M^{-1} (Table 1). Using PISA,[29] we determined the area of the dimer interface in the crystallographic structure of dPGM (715 Å^2 per monomer), and we predicted from the area that the *m*-value for dimer dissociation would be only 0.1 kcal mol^{-1} M^{-1} per monomer. The fact that $m_{I-N}/2$ (1.20 kcal mol^{-1} M^{-1}) is much greater than the value predicted for dimer dissociation suggests that the first transition involves not only dissociation of the dimer but also partial unfolding of the monomer. Further, m_{U-I} (1.86 kcal mol^{-1} M^{-1}) is much lower than the predicted *m*-value for unfolding of the monomer (3.2 kcal mol^{-1} M^{-1}), which clearly shows that the second transition cannot account for unfolding of an intact monomer. The spectroscopic signal of the intermediate state is distinct from the native state by both fluorescence and CD, which also supports a partially unfolded intermediate (Figure 1 and Figure S1).

Structural Determinant of Binding of ATP to dPGM. To elucidate the structural determinant of ATP for the

DOI: 10.1021/acs.biochem.5b00980
Biochemistry XXXX, XXX, XXX−XXX

interaction with dPGM, we monitored equilibrium unfolding of dPGM in the presence of 1.0 mM adenosine, AMP, ADP, or GTP (Figure 3A). While the effect of adenosine is negligible,

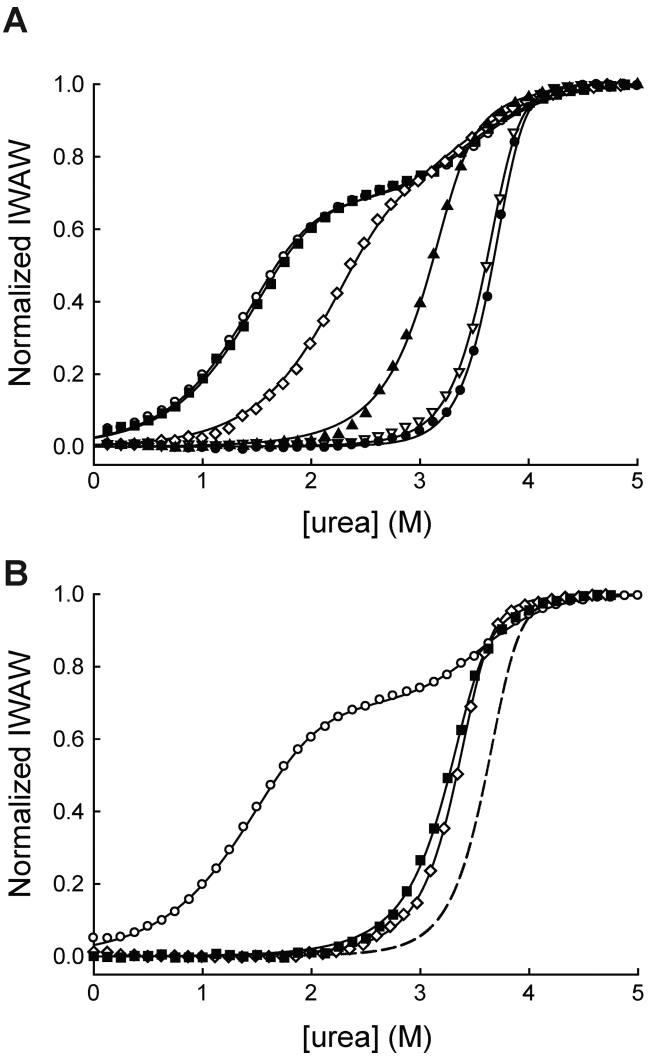

Figure 3. Effect of nucleotides on equilibrium unfolding of dPGM. (A) Equilibrium unfolding of 0.03 mg/mL dPGM was examined in buffer only (○) and in the presence of adenosine (■), AMP (◇), ADP (▲), ATP (▽), and GTP (●) each at 1.0 mM. The data were globally fit to eq 4 (—), and the fitting results are listed in Table 2. (B) Equilibrium unfolding of dPGM was also monitored in the presence of 0.050 M phosphate (◇) and 0.1 mM pyrophosphate (■). Both data sets and equilibrium unfolding data of dPGM without any ligand (○) were globally fit to eq 4 (—), and the fitting results are listed in Table 2. The fitting results for dPGM unfolding in the presence of ATP are shown as a dashed line for reference. For proper comparison, intensity-weighted average wavelengths (IWAWs) were normalized with eq 5.

AMP, ADP, and GTP significantly shift the first unfolding transition to higher urea concentrations. We fit globally the equilibrium unfolding data in Figure 3A, including equilibrium unfolding of dPGM in the absence and presence of 1.0 mM ATP, using the three-state model (Table 2). The data sets in the global fitting share the same *m*-values and spectroscopic signals for native, intermediate, and unfolded states. AMP, ADP, and GTP all stabilize the native form exclusively; while ΔG_{I-N}° increases dramatically, ΔG_{U-I}° is overall insensitive to the presence of the nucleotides. The change in ΔG_{I-N}° ($\Delta\Delta G_{I-N}^{\circ}$) is clearly dependent on the number of phosphate groups (Table 2); the more phosphate groups a nucleotide contains, the larger ΔG_{I-N}° becomes. ATP and GTP have similar effects on dPGM, suggesting that the type of the nucleobase is not important in the interaction. The stabilizing effects of this series of nucleotides show that the phosphate groups of nucleotides are the primary structural determinant of the interaction with dPGM.

The critical role of the phosphate groups in the interactions between nucleotides and dPGM led us to examine whether the same effect could be achieved by phosphate alone. We conducted equilibrium unfolding of dPGM in the presence of 50 mM phosphate or 0.10 mM pyrophosphate (Figure 3B). Both salts dramatically stabilize dPGM, and the equilibrium unfolding appears to be two-state. We fit globally the equilibrium unfolding data in the presence of either phosphate or pyrophosphate in pair with the equilibrium unfolding data of dPGM without any ligand (Table 2). The stabilizing effects of both ions are similar in spite of the 500-fold difference in concentration; 50 mM phosphate increased ΔG_{I-N}° by 5.9 kcal/mol, and 0.1 mM pyrophosphate increased ΔG_{I-N}° by 5.3 kcal/mol. Again, increasing the number of phosphates per molecule drastically increases the stability conveyed to dPGM. Interestingly, 0.1 mM pyrophosphate is as effective as 1.0 mM ADP in stabilizing dPGM, although pyrophosphate is present at a 10-fold lower concentration. The lack of the bulky nucleoside seems to enhance the binding affinity of pyrophosphate, which corroborates the finding that the nucleoside group (nucleobase and ribose) does not have any significant role in the interaction. Rather, ATP and other nucleotides bind to dPGM as a mono-, di-, or triphosphate, probably through Coulombic interactions with an extensive array of cationic residues of the protein. The potential binding site with this property is the active site of dPGM. As the crystal structure of dPGM reveals, the active site contains many basic residues in the proximity.[17] Moreover, the crystallographic structure of a complex between inactive dPGM and tetravanadate has shown that tetravanadate binds to the active site of the enzyme.[30] Therefore, binding of the triphosphate groups of ATP to the active site may mitigate unfavorable Coulombic interactions in the active site and stabilize the native form of dPGM.

Prediction of the ATP-Binding Site by Docking. To predict the ATP-binding site in dPGM, we docked ATP to dPGM using Maestro for Glide docking.[24] The docking grid was larger than one dPGM monomer to refrain from biasing the predicted binding site. As illustrated in Figure 4, ATP was predicted to bind to dPGM within the active site. Bound ATP is oriented with the adenosine moiety partially exposed to solvent and docked in the active-site opening, while the phosphate groups are sheltered within the active site. We identified potential hydrogen bond partners as donor−acceptor pairs separated by *d* with acceptable geometry, where 2.5 Å ≤ *d* ≤ 3.3 Å. The adenine of ATP can bond with only Asn16, and the ribose forms one bond with Lys238. The phosphate groups of ATP are predicted to form ion-pair hydrogen bonds with multiple residues. The *α*-phosphate group forms hydrogen bonds with Arg9, Lys99, Arg115, and Arg116. The *β*-phosphate group forms hydrogen bonds with Arg89, Tyr91, Lys99, Arg115, Arg116, and Asn185. Located the farthest into the active-site pocket, the *γ*-phosphate group can form hydrogen bonds with Gly23 and Lys99.

The predicted binding mode of ATP is analogous to the binding mode of the tetravanadate observed in the crystallo-

DOI: 10.1021/acs.biochem.5b00980
Biochemistry XXXX, XXX, XXX−XXX

Table 2. Thermodynamic Parameters of dPGM Unfolding in the Presence of Nucleotides and Phosphates

ligand	ΔG_{I-N}° (kcal/mol)	m_{I-N} (kcal mol^{-1} M^{-1})	ΔG_{U-I}° (kcal/mol)	m_{U-I} (kcal mol^{-1} M^{-1})	$\Delta\Delta G_{I-N}^{\circ}$[d] (kcal/mol)	K_d[e] (μM)
–[a]	11.6 ± 0.1	2.56 ± 0.03	5.6 ± 0.2	1.62 ± 0.05	–	–
adenosine[a]	11.7 ± 0.1	–	5.6 ± 0.2	–	0.09 ± 0.07	–
AMP[a]	13.6 ± 0.1	–	5.5 ± 0.2	–	1.96 ± 0.09	240 ± 40
ADP[a]	16.4 ± 0.1	–	5.2 ± 0.2	–	4.8 ± 0.1	18 ± 3
ATP[a]	19.3 ± 0.2	–	5.0 ± 0.3	–	7.7 ± 0.2	1.5 ± 0.5
GTP[a]	20.9 ± 0.8	–	4.3 ± 0.6	–	9.3 ± 0.8	0.4 ± 0.5
phosphate[b]	17.3 ± 0.1	2.36 ± 0.03	5.6 ± 0.3	1.82 ± 0.08	5.9 ± 0.1	350 ± 60
pyrophosphate[c]	16.8 ± 0.1	2.47 ± 0.04	5.2 ± 0.3	1.62 ± 0.09	5.3 ± 0.1	1.2 ± 0.2

[a]All data sets were fit with one global fit; all ligand concentrations were 1.0 mM. [b]Equilibrium unfolding data with 50 mM phosphate were fit globally along with equilibrium unfolding data without a ligand. [c]Equilibrium unfolding data with 0.10 mM pyrophosphate were fit globally along with equilibrium unfolding data without a ligand. [d]$\Delta\Delta G_{I-N}^{\circ} = \Delta G_{I-N}^{\circ}$(ligand) − ΔG_{I-N}°(no ligand). [e]K_d values were calculated with eq 6.

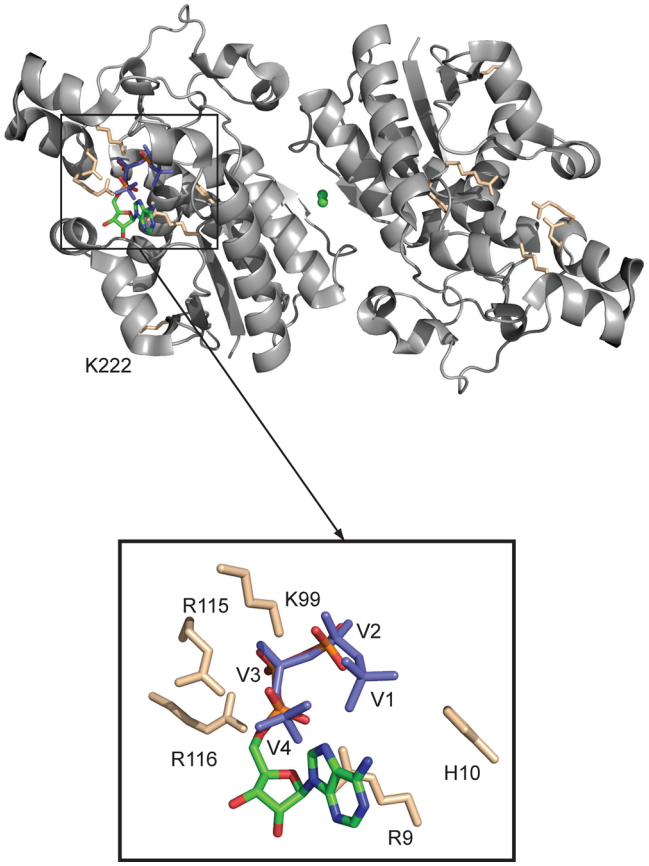

Figure 4. Predicted binding mode for ATP. ATP was docked to dPGM (PDB entry 1E59) using GLIDE. ATP is shown docked in one active site in the context of the full dPGM dimer. ATP is colored by element as follows: green for carbon, blue for nitrogen, orange for phosphate, and red for oxygen. In the dimer structure, a chloride ion (green) is bound within the dimer interface. A magnified view of the active site reveals that the phosphates of ATP occupy the same positions as vanadate groups of the tetravanadate (light blue) that is bound in the crystallographic structure. The side chains are displayed for residues Arg9, Lys99, Arg115, and Arg116, which are predicted to hydrogen bond with ATP. The active-site histidine (His10) and Lys222 are also shown for reference.

graphic structure of dPGM.[30] Tetravanadate bound in the active site, and the locations of the four vanadate groups were denoted as V1−V4.[30] Remarkably, the α-, β-, and γ-phosphates of ATP are predicted to be located approximately at V4, V3, and V2, respectively (Figure 4). Most of the predicted bonds between the phosphate groups of ATP and dPGM are also formed between tetravanadate and dPGM; only the α-phosphate group is predicted to form bonds that are not observed with tetravanadate. This difference likely arises because three oxygen atoms of the vanadate moiety were modeled as zero occupancy because of poor electron density.[30] The top four scoring poses from GLIDE were analyzed to test whether ATP is predicted to have multiple binding modes that are close in energy. Notably, the nucleoside moiety is predicted to adopt various conformations, while the top two scoring poses show complete overlap in the positions of the phosphate groups (Figure S3 of the Supporting Information). In the two less favorable poses, the α-, β-, and γ-phosphates are located at V3, V2, and V1, respectively. The agreement between the predicted binding mode of ATP and that of tetravanadate in the crystallographic structure of *E. coli* dPGM supports the idea that the predicted binding mode of ATP is viable.

Contribution of the Active-Site Residues to ATP Binding and Stability. To test the involvement of active-site residues in binding with ATP, we generated a series of dPGM variants with a point mutation to alanine at Arg9, Lys99, Arg115, and Arg116 (Figure 4). If a residue interacts with ATP through its side chain, an alanine mutation will abolish the interaction and result in ATP conferring less stability to that variant than to wild-type dPGM. As a control, we also mutated Lys222, which is distal to the active site (Figure 4), to alanine. CD spectra show that all the variants retain the secondary structure of wild-type dPGM (Figure S4 of the Supporting Information). We examined the equilibrium unfolding of each variant in the presence and absence of 1.0 mM ATP (Figure 5). To quantify the changes in stability conveyed to dPGM by ATP (ΔG_{ATP}°), we fit globally each variant in the presence and absence of 1.0 mM ATP using the three-state model represented in Scheme 1 (Table 3). Because ATP stabilizes only native dPGM, we define ΔG_{ATP}° as ΔG_{I-N}(ATP)° − ΔG_{I-N}°.

As with wild-type dPGM, the equilibrium unfolding of each variant appears to be three-state. Effects of R9A and K222A mutations on equilibrium unfolding were insignificant (Figure 5A,E). However, K99A, R115A, and R116A mutations all shift the first transition to urea concentrations higher than that observed with wild-type dPGM. This indicates that K99A, R115A, and R116A mutations stabilize the native state alone. K99A (Figure 5B), R115A (Figure 5C), and R116A (Figure 5D) mutations increase ΔG_{I-N}° by 2.3 ± 0.2, 3.1 ± 0.3, and 1.2 ± 0.1 kcal/mol, respectively. No mutations alter the stability of **I** significantly.

In the presence of 1.0 mM ATP, the stability of all variants is dramatically increased (Figure 5). For each active-site variant,

DOI: 10.1021/acs.biochem.5b00980
Biochemistry XXXX, XXX, XXX−XXX

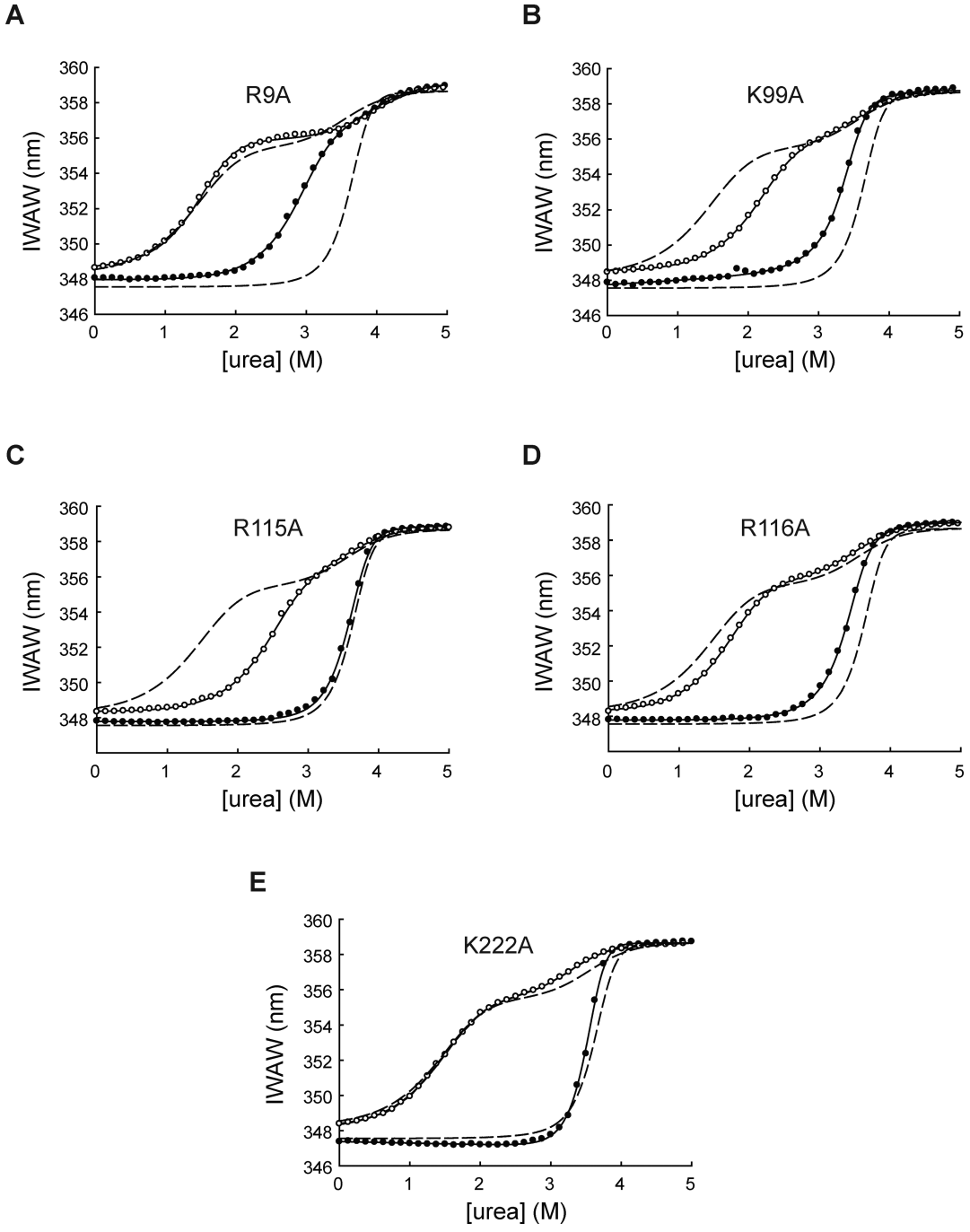

Figure 5. Effect of dPGM point mutations on the stabilizing effect of ATP. Equilibrium unfolding of 0.03 mg/mL (A) R9A, (B) K99A, (C) R115A, (D) R116A, and (E) K222A in the presence (●) and absence (○) of 1.0 mM ATP. The fit lines of wild-type dPGM in the presence and absence of ATP are shown (– – –) for reference.

ΔG_{ATP}° is less than that of the wild type (7.0 kcal/mol). The R116A variant gains the most stability from ATP with a ΔG_{ATP}° of 5.4 ± 0.2 kcal/mol. R9A and K99A are the least stabilized by 1.0 mM ATP with ΔG_{ATP}° values of 4.2 ± 0.2 and 4.0 ± 0.4 kcal/mol, respectively. With R115A, ΔG_{ATP}° is 4.8 ± 0.4 kcal/mol. Notably, the intermediate is still apparent for R9A in the presence of 1.0 mM ATP because of the rightward shift of its second unfolding transition. The control mutation, K222A, does not appear to significantly influence the stabilizing effect of ATP (Figure 5E). Because the active-site mutations reduce ΔG_{ATP}° while the control does not, ATP clearly interacts with the active-site residues.

The effects of the active-site mutations on native dPGM (N_2) and the intermediate form (I) betray conformational differences between the two forms. If the environment of the mutated active-site residues was similar in both N_2 and I, then removal of the side chain would stabilize I in a manner similar to that of N_2. The K99A, R115A, and R116A mutations stabilize N_2, which is evident by the increase in ΔG_{I-N}°, but had insignificant effects on the second transition (Table 3). The selective enhancement of ΔG_{I-N}° suggests that Lys99, Arg115, and Arg116 are in an unfavorable environment for N_2 and that removal of the positive charges from the active site stabilizes the protein similar to phosphate binding. Because removal of

DOI: 10.1021/acs.biochem.5b00980
Biochemistry XXXX, XXX, XXX−XXX

Table 3. Thermodynamic Parameters of dPGM Variants in the Presence and Absence of ATP

variant	[ATP] (mM)	ΔG_{I-N}° (kcal/mol)	m_{I-N} (kcal mol^{-1} M^{-1})	ΔG_{U-I}° (kcal/mol)	m_{U-I} (kcal mol^{-1} M^{-1})	ΔG_{ATP}°[a] (kcal/mol)
R9A	0	12.4 ± 0.1	2.98 ± 0.07	6.4 ± 0.5	1.6 ± 0.1	
	1.0	16.6 ± 0.2	–	6.3 ± 0.5	–	4.2 ± 0.2
K99A	0	13.8 ± 0.2	2.70 ± 0.08	7 ± 1	1.9 ± 0.3	
	1.0	18.5 ± 0.2	–	6 ± 1	–	4.0 ± 0.4
R115A	0	14.6 ± 0.3	2.7 ± 0.1	5 ± 1	1.5 ± 0.3	
	1.0	19.4 ± 0.3	–	5 ± 1	–	4.8 ± 0.4
R116A	0	12.71 ± 0.09	2.75 ± 0.05	6.0 ± 0.4	1.7 ± 0.1	
	1.0	18.1 ± 0.2	–	5.8 ± 0.4	–	5.4 ± 0.2
K222A	0	11.6 ± 0.1	2.48 ± 0.09	6.1 ± 0.4	1.9 ± 0.1	
	1.0	21 ± 2	–	4.4 ± 0.9	–	9 ± 2

[a] $\Delta G_{ATP}^{\circ} = \Delta G_{I-N}^{\circ}$(1 mM ATP) − ΔG_{I-N}°(no ATP).

Lys99, Arg115, or Arg116 does not alter the stability of I, the environment the residues experience in I is quite distinct from that in N_2. Collectively, the effects of point mutations on the equilibrium unfolding of dPGM support a model in which the active site is disrupted in the monomeric intermediate state.

Validation of the ATP-Interacting Residues by Isothermal Titration Calorimetry. ATP binding by each dPGM variant was monitored using isothermal titration calorimetry (ITC) to obtain the dissociation equilibrium constant, K_d (Table 4 and Figure S5 of the Supporting Information). Wild-type dPGM was found to bind ATP with a K_d of 0.32 ± 0.07 μM. R116A retained the greatest affinity for ATP out of the active-site mutants with a K_d of 1.5 ± 0.3 μM. The variants with the most jeopardized ATP binding are K99A and R115A, which have K_d values of 7 ± 2 μM. For R9A, K_d is 5.5 ± 0.05 μM. As anticipated, K222A has a negligible impact on ATP binding with a K_d of 0.4 ± 0.1 μM. The K_d value determined for each active-site mutant is increased relative to that of wild-type dPGM, which signifies the role of the residues in ATP binding. The effects of mutation on K_d confirm that each active-site residue chosen for mutation is involved in ATP binding while the control is not.

Table 4. ATP Binding Monitored by ITC

variant	K_d (×10^{-6} M)	ΔG_{bind}°[a] (kcal/mol)	$\Delta\Delta G_{bind}^{\circ}$[b] (kcal/mol)	$\Delta\Delta G_{ATP}^{\circ}$[c] (kcal/mol)
WT	0.32 ± 0.07	4.7 ± 0.1		
R9A	5.5 ± 0.5	3.1 ± 0.05	−1.7 ± 0.1	−1.4 ± 0.1
K99A	7 ± 2	2.9 ± 0.2	−1.8 ± 0.2	−1.5 ± 0.2
R115A	7 ± 2	2.9 ± 0.2	−1.8 ± 0.2	−1.1 ± 0.2
R116A	1.5 ± 0.3	3.8 ± 0.1	−0.9 ± 0.2	−0.8 ± 0.1
K222A	0.4 ± 0.1	4.6 ± 0.1	−0.1 ± 0.2	1.2 ± 1

[a] ΔG_{bind}° was calculated with eq 6 using 1.0 mM ATP. [b] $\Delta\Delta G_{bind}^{\circ} = \Delta G_{bind}^{\circ}$(variant) − ΔG_{bind}°(WT). [c] $\Delta\Delta G_{ATP}^{\circ} = \Delta G_{ATP}^{\circ}$(variant) − ΔG_{ATP}°(WT).

From the K_d values, we calculated the free energy change for binding, ΔG_{bind}°, at 1.0 mM ATP (Table 4). The effect of a mutation on ΔG_{bind}° ($\Delta\Delta G_{bind}^{\circ}$) should be the same as the effect of the mutation on ΔG_{ATP}° ($\Delta\Delta G_{ATP}^{\circ}$) determined from equilibrium unfolding if our model (Scheme 1) is correct. As shown in Table 4, the $\Delta\Delta G_{bind}^{\circ}$ and $\Delta\Delta G_{ATP}^{\circ}$ values are similar for the active-site variants, although $\Delta\Delta G_{bind}^{\circ}$ values are consistently greater in magnitude than the $\Delta\Delta G_{ATP}^{\circ}$ values. This difference may arise from the effect of urea on ATP binding because we calculated $\Delta\Delta G_{ATP}^{\circ}$ values from equilibrium unfolding in urea. Overall, the effect of the mutations as determined by ITC corroborates what we determined from the equilibrium unfolding study. The agreement between the two techniques also verifies that the three-state model applied to equilibrium unfolding is appropriate in the presence and absence of 1.0 mM ATP.

DISCUSSION

We demonstrated that equilibrium unfolding of dPGM occurs in a three-state manner with a monomeric intermediate (Figure 1A). The *m*-values and the spectroscopic signals indicate that the monomeric intermediate is partially unfolded. In the presence of ATP, the monomeric intermediate is barely populated throughout equilibrium unfolding (Figure 1B). Through an increase in ΔG_{I-N}°, 1.0 mM ATP nearly shifts the equilibrium unfolding of dPGM into a two-state folding system where the entire protein is either folded or unfolded. Using a computational modeling and site-directed mutagenesis, we also clearly demonstrated that ATP binds to the active site of the enzyme through the interactions between cationic residues in the active site and the triphosphate group of ATP. During catalysis, the active site of dPGM accommodates the substrates (2-phosphoglycerate and 3-phosphoglycerate) or the cofactor (2,3-bisphosphoglycerate). Apparently, the triphosphate group of ATP mimics the multianionic structures of the substrates and the cofactor. Though we identified dPGM as an ATP-binding protein in our previous proteomics screen, the interaction is not specific to ATP. Any ligand with repeating phosphate groups such as ADP, GTP, or pyrophosphate can bind to the active site with significant affinity. In this study, we investigated the binding of ATP to dPGM under a low-salt condition to reliably assess the contribution of ligand binding to the folding of the protein. Because the interaction between ligands with phosphoryl groups and dPGM is mostly Coulombic, the affinity of the ligands for the protein is reduced under physiological salt conditions (N. W. Gardner and C. Park, unpublished results). Still, the total concentration of the metabolites with diphosphate or triphosphate groups can be tens of millimolar in the cellular environment, and these functionally unrelated metabolites may significantly influence the stability of dPGM. Further studies would be necessary to elucidate the role of the interaction between the metabolites and dPGM under physiological conditions

Ligand binding to dPGM selectively stabilizes the native dimer over a partially unfolded monomeric intermediate. Our analysis of equilibrium unfolding of dPGM in the presence of various ligands indicates that the ligands do not stabilize the monomeric intermediate; the effects of ligands on ΔG_{U-I}° are all negligible (Tables 1 and 2). The lack of stabilization by the

DOI: 10.1021/acs.biochem.5b00980
Biochemistry XXXX, XXX, XXX−XXX

ligands suggests that the active site is disrupted in the monomeric intermediate. The effect of active-site mutations on stability also suggests that the active site is unfolded in the intermediate. Therefore, dissociation of the dimer into the monomeric intermediate also induces unfolding of the active site. The active site of dPGM is distal from the dimer interface (Figure 4), yet proper folding of the active site and the dimer interface appears to be cooperative.

A thermodynamic cycle clearly illustrates the cooperativity between ligand binding and dimerization in dPGM (Figure 6).

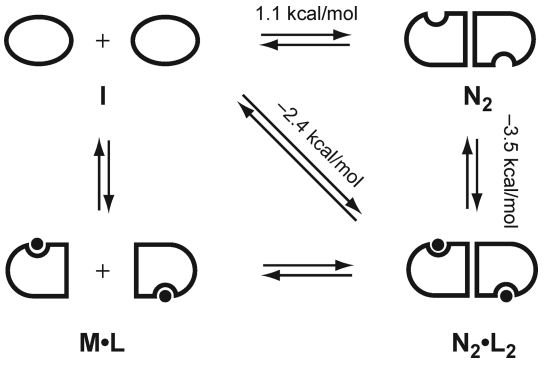

Figure 6. Mechanistic model for the energetic coupling of the dPGM active site and dimer interface. A simple thermodynamic cycle (A) illustrates the energetic coupling in dPGM. Apo dPGM exchanges between the intermediate state (I) and the native state (N_2). ATP binds to native dPGM ($N_2{\cdot}L_2$) and reduces its free energy. If the dPGM active site were not energetically coupled to the interface, dPGM might form an ATP-bound, folded monomer (M·L). The energetic penalty incurred for forming M·L ensures that dimerization and active-site formation will occur together.

In 2.5 M urea, where the cooperativity is most evident, dPGM is predominantly partially unfolded monomers (I) in the absence of ATP but ATP-bound dimers ($N_2{\cdot}L_2$) in the presence of 1.0 mM ATP (Figure 1). The reaction from I to $N_2{\cdot}L_2$ is thermodynamically favorable in the presence of 1.0 mM ATP. The free energy change associated with the reaction from I to $N_2{\cdot}L_2$ in 2.5 M urea can be calculated using the thermodynamic parameters of equilibrium unfolding in Table 1 and eq 2 ($\Delta G_{N-I}^{\circ} = -12.5$ kcal/mol). Under our experimental condition (1 μM dPGM), the ΔG_{N-I}° value corresponds to the effective free energy change[27] of −2.4 kcal/mol per monomer, which is consistent with the reaction from I to $N_2{\cdot}L_2$ being thermodynamically favorable. The predominant presence of I in the absence of ATP indicates that dimerization of the partially unfolded monomer (I to N_2) is thermodynamically unfavorable at 2.5 M urea. The free energy change associated with the reaction from I to N_2 is again calculated using the thermodynamic parameters of equilibrium unfolding in Table 1 and eq 2 ($\Delta G_{N-I}^{\circ} = -5.5$ kcal/mol). Under our experimental condition (1 μM dPGM), the effective free energy change[27] of the reaction is 1.1 kcal/mol per monomer, which again confirms that folding of I to N_2 is unfavorable under this condition. Then, the thermodynamic relationship shows that binding of ATP to the native dimer (N_2) is associated with a ΔG° of −3.5 kcal/mol in the presence of 1.0 mM ATP. The favorable binding energy by ATP (−3.5 kcal/mol per monomer) overcomes the unfavorable free energy associated with the folding and dimerization (1.1 kcal/mol per monomer). The affinity to ATP is enhanced significantly because the formation of N_2 already pays the penalty of forming the binding-competent active site. This phenomenon is, therefore, an example of preorganization of the binding site.

The energetics of the same reaction can be analyzed through the pathway with ligand-bound folded monomer (M·L). As we cannot observe M·L under any circumstance, we do not have thermodynamic data for this pathway. However, the cooperative nature between ligand binding and dimerization can be explained with this pathway also. The dimerization of M·L to $N_2{\cdot}L_2$ must be thermodynamically favorable, because the free energy change associated with this reaction is the inverse of the energetic penalty (Δg_{int}) of exposing the dimer interface to the solvent. Therefore, ligand binding drives the folding of the monomer (I to M·L), which is followed by a favorable dimerization reaction. This scenario can be seen as a cooperative binding between two ligands. Binding of one ligand (L) promotes the folding of the other binding site (the dimer interface), which dramatically increases the affinity for the other ligand (another monomeric unit).

The ligand-induced dimerization of dPGM in 2.5 M urea is reminiscent of allostery observed in proteins with an intrinsically unstructured region. Maximal energetic coupling between two domains or regions is achieved when a segment of the protein is folded only in the presence of ligand and when abolishing the interaction between the domains causes a large energetic penalty.[6,31] dPGM in 2.5 M urea satisfies these conditions. The active site and the dimer interface fold only when a ligand is present. Also, exposing the dimer interface is significantly unfavorable. Also of note is the fact that the energetic coupling in dPGM should allow ligand binding to one subunit to bolster the stability of the other subunit through the dimer interface, which will lead to favorable binding of ligand to the other subunit. Though the cooperativity is most dramatic in 2.5 M urea, the energetic coupling between the active site and the dimer interface exists under native conditions also. f_I is significantly decreased in the presence of 1.0 mM ATP (Figure 1B). We expect that phosphorylation of His10 and/or substrate binding in one subunit will alleviate Columbic strain in the active site and stabilize the dimeric form, which will lead to the stabilization of the other subunit, as well.

The crystallographic structure of dPGM offers clues about how the active site may be structurally coupled to the dimer interface. A loop comprising residues 118−151 leads from the active site of dPGM to the dimer interface with portions of the loop making intersubunit contacts (Figure 7). The loop connects helix α5 (residues 108−117), which forms part of the active-site rim and contains Arg115 and Arg116, to helix α6 (residues 152−167) (Figure 7). If the active-site structure were disrupted, unfolding of helix α5 may increase the dynamics of the adjacent loop; likewise, ligand binding to residues Arg115 and Arg116 could anchor helix α5 and reduce the dynamics of the adjacent loop and, consequently, stabilize the dimer interface. Interestingly, Arg115 interacts with the C-terminal tail of dPGM, which folds over the active site, when the enzyme is phosphorylated.[17] Arg115 and Arg116 have been postulated to play a main role in switching between inactive and active conformations due to substrate binding.[17] These two substrate-binding residues appear to be a hot spot for energetically linking the active site to structural change throughout the protein.

The sequence, secondary structure, and active-site structure of dPGM are well conserved across *E. coli*, *S. cerevisiae*, *Schizosaccharomyces pombe*, and human brain dPGM, with the key differences being localized to subunit interfaces.[17] Despite

DOI: 10.1021/acs.biochem.5b00980
Biochemistry XXXX, XXX, XXX−XXX

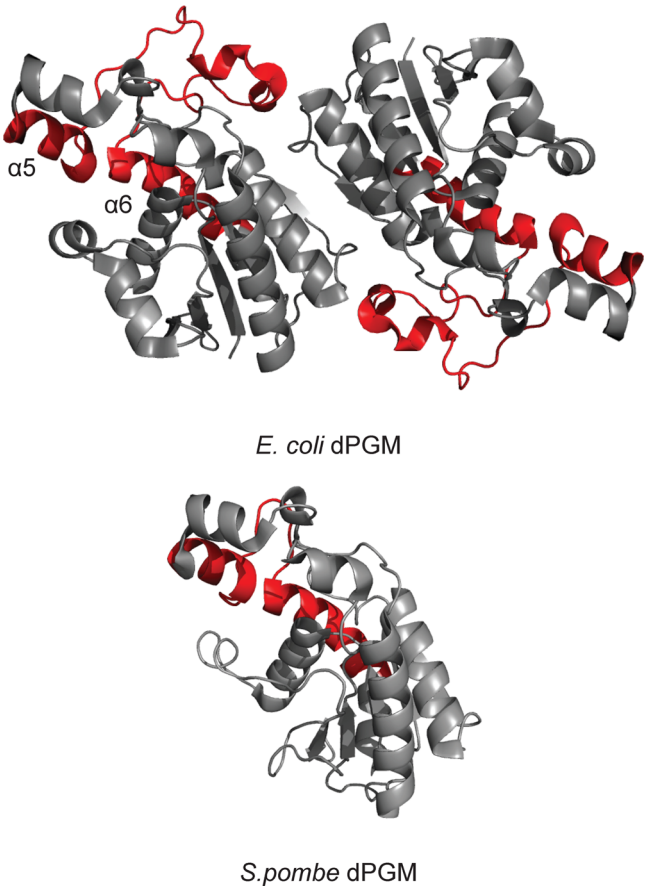

Figure 7. Putative structural link between the active site and the dimer interface. The cartoon representation of the crystallographic structure of *E. coli* dPGM (PDB entry 1E59) is shown with a plausible structural link (red) between the active site and the dimer interface. A long loop leads from active-site helix α5 to the dimer interface and then to helix α6. For comparison, the equivalent region is shown in a cartoon representation of the solution structure of *Schizosaccharomyces pombe* dPGM (PDB entry 1FZT), which is a monomeric protein.

the high degree of sequence similarity between homologous dPGMs, *E. coli* and mammalian dPGMs are dimeric, *S. cerevisiae* dPGM is tetrameric, and *S. pombe* dPGM is monomeric.[17] Like *E. coli* dPGM, oligomeric human and *S. cerevisiae* dPGMs have a "split" helix (α5/α6) with a long loop from helix α5 to helix α6 that takes part in intersubunit contacts.[32,33] However, the monomeric *S. pombe* dPGM contains a drastically truncated loop, 25 residues shorter than the loop in *E. coli* dPGM, which would not be able to take part in the dimer interface (Figure 7).[34,35] The absence of this long loop in the monomeric *S. pombe* dPGM suggests to us that the loop indeed provides a key structural link between the active site and subunit interface that drives the energetic coupling we observed. We are currently determining the structure of the monomeric intermediate of *E. coli* dPGM, which may elucidate the structural link between the active site and dimer interface.

The energetic coupling between ligand binding and the dimerization in dPGM is consistent with the findings from computational studies that active-site residues tend to have greater energetic coupling with other regions of a protein.[36,37] A survey of 16 proteins revealed that active sites tend to contain low-stability regions that rearrange in the presence of ligand and underlie high-affinity binding.[36] When the active sites unfold, conformational changes tend to propagate throughout the protein, not simply in the vicinity of the active site.[36] These low-stability active-site regions are then energetically linked with a significant portion of the protein structure.[38] A rigorous analysis of the energetic coupling between regions in the structures of five monomeric proteins revealed that active sites contain the residues with the greatest amount of energetic coupling to other regions of the protein; active sites exert the greatest control over the conformational ensemble.[37]

The effect of ATP and other stabilizing ligands on dPGM shows that cooperativity between ligand binding and dimerization may suppress dissociation of a dimer in the presence of ligand. This principle can be extended to multimeric proteins, as well. In a multimeric protein, oligomerization can be energetically coupled with the folding of a distal active site and also ligand binding at the active site. The active site and the dimer interface of dPGM show positive cooperativity so that the two different regions fold and unfold in concert. The resulting effect of the positive cooperativity is that ligand binding stabilizes only the native multimeric forms and redistributes the ensemble populations away from partially unfolded monomeric forms. Increasing the energy gap between the native protein and partially unfolded conformations is paramount to avoiding risky partial unfolding, which can lead to proteolytic digestion,[39] misfolding,[40] and aggregation[41] and might cause disease states.[42] In principle, negative cooperativity is also possible in multimeric proteins. In this case, ligand binding is coupled with unfolding of the interface, which promotes the dissociation of multimeric proteins. One seminal example of negative cooperativity is the release of the two active monomers of protein kinase A from the heterotetrameric complex with two regulatory subunits upon binding of cAMP to the regulatory subunits.[43] Exploiting and imitating energetic coupling between ligand binding and multimerization would be valuable in designing and engineering novel proteins not only with desired structures but also with useful regulatory mechanisms.

■ ASSOCIATED CONTENT

Supporting Information

The Supporting Information is available free of charge on the ACS Publications website at DOI: 10.1021/acs.biochem.5b00980.

Equilibrium unfolding of dPGM monitored by circular dichroism (Figure S1); The concentration dependence of equilibrium unfolding of dPGM monitored by circular dichroism (Figure S2); Comparison of the four most favorable poses of ATP docked to dPGM (Figure S3); Circular dichroism spectra of the dPGM variants (Figure S4); Thermograms for ATP binding to dPGM determined by isothermal titration calorimetry (Figure S5). (PDF)

■ AUTHOR INFORMATION

Corresponding Author

*E-mail: chiwook@purdue.edu. Telephone: 1-765-496-7513. Fax: 1-765-494-1414.

Funding

The work was funded by National Institutes of Health Grant GM097528. N.W.G. was also partly supported by the McKeehan Graduate Fellowship from the College of Pharmacy, Purdue University.

DOI: 10.1021/acs.biochem.5b00980
Biochemistry XXXX, XXX, XXX−XXX

Notes

The authors declare no competing financial interest.

■ ACKNOWLEDGMENTS

We thank Dr. Lake Paul (Bindley Bioscience Center, Purdue University) for conducting the isothermal titration calorimetry experiments and analysis and Dr. Elizabeth Topp and the Topp laboratory for sharing their HPLC and CD spectrometer. We also thank Dr. Nathalie Declerck (Centre de Biochimie Structural, Montpellier, France) for her insightful suggestions regarding the structural interpretation of our results upon reviewing our original manuscript submitted for publication. We also thank Chen Chen for her useful commentary on the manuscript.

■ ABBREVIATIONS

dPGM, *E. coli* cofactor-dependent phosphoglycerate mutase; AMP, adenosine monophosphate; ADP, adenosine diphosphate; ATP, adenosine triphosphate; GTP, guanosine triphosphate; CD, circular dichroism; IWAW, intensity-weighted average wavelength; ITC, isothermal titration calorimetry.

■ REFERENCES

(1) Freire, E., and Murphy, K. P. (1991) Molecular basis of cooperativity in protein folding. *J. Mol. Biol. 222*, 687−698.
(2) Bai, Y., Sosnick, T. R., Mayne, L., and Englander, S. W. (1995) Protein folding intermediates: Native-state hydrogen exchange. *Science 269*, 192−197.
(3) Chamberlain, A. K., Handel, T. M., and Marqusee, S. (1996) Detection of rare partially folded molecules in equilibrium with the native conformation of RNase H. *Nat. Struct. Biol. 3*, 782−787.
(4) Hu, W., Walters, B. T., Kan, Z. Y., Mayne, L., Rosen, L. E., Marqusee, S., and Englander, S. W. (2013) Stepwise protein folding at near amino acid resolution by hydrogen exchange and mass spectrometry. *Proc. Natl. Acad. Sci. U. S. A. 110*, 7684−7689.
(5) Motlagh, H. N., Wrabl, J. O., Li, J., and Hilser, V. J. (2014) The ensemble nature of allostery. *Nature 508*, 331−339.
(6) Hilser, V. J., and Thompson, E. B. (2007) Intrinsic disorder as a mechanism to optimize allosteric coupling in proteins. *Proc. Natl. Acad. Sci. U. S. A. 104*, 8311−8315.
(7) Luque, I., Leavitt, S. A., and Freire, E. (2002) The linkage between protein folding and functional cooperativity: two sides of the same coin? *Annu. Rev. Biophys. Biomol. Struct. 31*, 235−256.
(8) Chang, Y., Schlebach, J. P., VerHeul, R. A., and Park, C. (2012) Simplified proteomics approach to discover protein-ligand interactions. *Protein Sci. 21*, 1280−1287.
(9) Liu, P.-F., Kihara, D., and Park, C. (2011) Energetics-based discovery of protein-ligand interactions on a proteomic scale. *J. Mol. Biol. 408*, 147−162.
(10) Schellman, J. A. (1976) The effect of binding on the melting temperature of biopolymers. *Biopolymers 15*, 999−1000.
(11) Waldron, T. T., and Murphy, K. P. (2003) Stabilization of proteins by ligand binding: Application to drug screening and determination of unfolding energetics. *Biochemistry 42*, 5058−5064.
(12) Sanchez-Ruiz, J. M. (2007) Ligand effects on protein thermodynamic stability. *Biophys. Chem. 126*, 43−49.
(13) Park, C., and Marqusee, S. (2005) Pulse proteolysis: A simple method for quantitative determination of protein stability and ligand binding. *Nat. Methods 2*, 207−212.
(14) Adhikari, J., and Fitzgerald, M. C. (2014) SILAC-pulse proteolysis: A mass spectrometry-based method for discovery and cross-validation in proteome-wide studies of ligand binding. *J. Am. Soc. Mass Spectrom. 25*, 2073−2083.
(15) Chang, Y., Schlebach, J., VerHeul, R., and Park, C. (2012) Simplified proteomics approach to discover protein-ligand interactions. *Protein Sci. 21*, 1280−1287.
(16) Tran, D. T., Adhikari, J., and Fitzgerald, M. C. (2014) Stable Isotope Labeling with Amino Acids in Cell Culture (SILAC)-based strategy for proteome-wide thermodynamic analysis of protein-ligand binding interactions. *Mol. Cell. Proteomics 13*, 1800−1813.
(17) Bond, C., White, M., and Hunter, W. (2001) High resolution structure of the phosphohistidine-activated form of *Escherichia coli* cofactor-dependent phosphoglycerate mutase. *J. Biol. Chem. 276*, 3247−3253.
(18) Pace, C. N., Vajdos, F., Fee, L., Grimsley, G., and Gray, T. (1995) How to measure and predict the molar absorption coefficient of a protein. *Protein Sci. 4*, 2411−2423.
(19) Pace, C. N. (1986) Determination and analysis of urea and guanidine hydrochloride denaturation curves. *Methods Enzymol. 131*, 266−280.
(20) Gloss, L. M., and Matthews, C. R. (1997) Urea and thermal equilibrium denaturation studies on the dimerization domain of *Escherichia coli* Trp repressor. *Biochemistry 36*, 5612−5623.
(21) Mallam, A., and Jackson, S. (2005) Folding studies on a knotted protein. *J. Mol. Biol. 346*, 1409−1421.
(22) Greene, R. F., and Pace, C. N. (1974) Urea and guanidine-hydrochloride denaturation of ribonuclease, lysozyme, a-chymotrypsin, and b-lactoglobulin. *J. Biol. Chem. 249*, 5388−5393.
(23) Schellman, J. A. (1975) Macromolecular Binding. *Biopolymers 14*, 999−1018.
(24) Friesner, R. A., Banks, J. L., Murphy, R. B., Halgren, T. A., Klicic, J. J., Mainz, D. T., Repasky, M. P., Knoll, E. H., Shelley, M., Perry, J. K., Shaw, D. E., Francis, P., and Shenkin, P. S. (2004) Glide: A new approach for rapid, accurate docking and scoring. 1. Method and assessment of docking accuracy. *J. Med. Chem. 47*, 1739−1749.
(25) Keller, S., Vargas, C., Zhao, H., Piszczek, G., Brautigam, C., and Schuck, P. (2012) High-precision isothermal titration calorimetry with automated peak-shape analysis. *Anal. Chem. 84*, 5066−5073.
(26) Zhao, H., Piszczek, G., and Schuck, P. (2015) SEDPHAT − A platform for global ITC analysis and global multi-method analysis of molecular interactions. *Methods 76*, 137−148.
(27) Park, C., and Marqusee, S. (2004) Analysis of the stability of multimeric proteins by effective ΔG and effective *m*-values. *Protein Sci. 13*, 2553−2558.
(28) Myers, J. K., Pace, C. N., and Scholtz, J. M. (1995) Denaturant *m* values and heat capacity changes: Relation to changes in accessible surface areas of protein unfolding. *Protein Sci. 4*, 2138−2148.
(29) Krissinel, E., and Henrick, K. (2007) Inference of macromolecular assemblies from crystalline state. *J. Mol. Biol. 372*, 774−797.
(30) Bond, C., White, M., and Hunter, W. (2002) Mechanistic implications for *Escherichia coli* cofactor-dependent phosphoglycerate mutase based on the high-resolution crystal structure of a vanadate complex. *J. Mol. Biol. 316*, 1071−1081.
(31) Wrabl, J. O., Gu, J., Liu, T., Schrank, T. P., Whitten, S. T., and Hilser, V. J. (2011) The role of protein conformational fluctuations in allostery, function, and evolution. *Biophys. Chem. 159*, 129−141.
(32) Wang, Y., Wei, Z., Liu, L., Cheng, Z., Lin, Y., Ji, F., and Gong, W. (2005) Crystal structure of human B-type phosphoglycerate mutase bound with citrate. *Biochem. Biophys. Res. Commun. 331*, 1207−1215.
(33) Rigden, D. J., Walter, R. A., Phillips, S. E. V., and Fothergill-Gilmore, L. A. (1999) Sulphate ions observed in the 2.12 Å structure of a new crystal form of *S. cerevisiae* phosphoglycerate mutase provide insights into understanding the catalytic mechanism1. *J. Mol. Biol. 286*, 1507−1517.
(34) Nairn, J., Price, N. C., Fothergill-Gilmore, L. A., Walker, G. E., Fothergill, J. E., and Dunbar, B. (1994) The amino acid sequence of the small monomeric phosphoglycerate mutase from the fission yeast *Schizosaccharomyces pombe*. *Biochem. J. 297*, 603−608.
(35) Uhrínová, S., Uhrín, D., Nairn, J., Price, N. C., Fothergill-Gilmore, L. A., and Barlow, P. N. (2001) Solution structure and dynamics of an open β-sheet, glycolytic enzyme, monomeric 23.7 kDa phosphoglycerate mutase from *Schizosaccharomyces pombe*. *J. Mol. Biol. 306*, 275−290.

DOI: 10.1021/acs.biochem.5b00980
Biochemistry XXXX, XXX, XXX−XXX

(36) Luque, I., and Freire, E. (2000) Structural stability of binding sites: Consequences for binding affinity and allosteric effects. *Proteins: Struct., Funct., Genet. 41*, 63−71.
(37) Liu, T., Whitten, S. T., and Hilser, V. J. (2007) Functional residues serve a dominant role in mediating the cooperativity of the protein ensemble. *Proc. Natl. Acad. Sci. U. S. A. 104*, 4347−4352.
(38) Hilser, V. J., Dowdy, D., Oas, T. G., and Freire, E. (1998) The structural distribution of cooperative interactions in proteins: Analysis of the native state ensemble. *Proc. Natl. Acad. Sci. U. S. A. 95*, 9903−9908.
(39) Hubbard, S. J. (1998) The structural aspects of limited proteolysis of native proteins. *Biochim. Biophys. Acta, Protein Struct. Mol. Enzymol. 1382*, 191−206.
(40) Dobson, C. M. (2003) Protein folding and misfolding. *Nature 426*, 884−890.
(41) Horwich, A. (2002) Protein aggregation in disease: A role for folding intermediates forming specific multimeric interactions. *J. Clin. Invest. 110*, 1221−1232.
(42) Thomas, P. J., Qu, B.-H., and Pedersen, P. L. (1995) Defective protein folding as a basis of human disease. *Trends Biochem. Sci. 20*, 456−459.
(43) Taylor, S. S., Buechler, J. A., and Yonemoto, W. (1990) cAMP-dependent protein kinase: framework for a diverse family of regulatory enzymes. *Annu. Rev. Biochem. 59*, 971−1005.

DOI: 10.1021/acs.biochem.5b00980
Biochemistry XXXX, XXX, XXX−XXX